RMetS
Royal Meteorological Society

Increase in the skewness of extratropical vertical velocities with climate warming: fully nonlinear simulations versus moist baroclinic instability

Paul A. O'Gorman,[a]* Timothy M. Merlis[b] and Martin S. Singh[c]

[a]*Department of Earth, Atmospheric and Planetary Sciences, Massachusetts Institute of Technology, USA*
[b]*Department of Atmospheric and Oceanic Sciences, McGill University, Québec, Canada*
[c]*School of Earth, Atmosphere and Environment, Monash University, Victoria, Australia*

*Correspondence to: P. A. O'Gorman, Department of Earth, Atmospheric and Planetary Sciences, MIT, Cambridge MA 02139, USA.
E-mail: pog@mit.edu

The distribution of vertical velocities in the extratropical troposphere is skewed such that upward motions are faster than downward motions. This skewness is important for the intensity distribution of precipitation and for the effective static stability experienced by moist eddies. We show here that the skewness of the vertical velocity increases in magnitude as the climate warms in simulations with an idealized general circulation model (GCM), except in very warm climates. That the skewness increases with warming is consistent with studies of moist baroclinic instability which suggest that the area of updraughts should contract as the stratification approaches moist neutrality in warm climates. However, the increase in skewness with warming is much weaker in the fully nonlinear simulations as compared to what is found for unstable modes of moist baroclinic instability in the same GCM. Nonlinear equilibration to a macroturbulent state leads to a reduction in skewness in warm climates. Therefore, while the unstable modes may be relevant for some cases of cyclogenesis, they overestimate the effect of warming on the skewness of the overall distribution of the vertical velocity. Remarkably, the most unstable mode transitions from a quasi-periodic wave to an isolated diabatic Rossby vortex at sufficiently high temperatures, with possible implications for fast-growing disturbances in warm climates.

Key Words: skewness; vertical velocity; non-Gaussian; moist baroclinic instability; diabatic Rossby vortex; diabatic Rossby wave; effective static stability; climate change

Received 20 March 2017; Revised 15 September 2017; Accepted 23 October 2017; Published online in Wiley Online Library 27 December 2017

1. Introduction

The distribution of tropospheric vertical velocities is not Gaussian, but rather it is skewed in a way that tends to make upward velocities stronger than downward velocities. This skewness is found for both large-scale vertical velocities from reanalysis (e.g. Perron and Sura, 2013) and smaller-scale convective vertical velocities (e.g. Moeng and Rotunno, 1990). Here we will focus on large-scale vertical velocities in the extratropical troposphere as measured by the negative of the vertical velocity ω in pressure coordinates, such that positive values are upwards. The skewness of $-\omega$ is defined as

$$\text{skewness} = -\frac{\overline{\omega'^3}}{(\overline{\omega'^2})^{3/2}}, \qquad (1)$$

where the overbar denotes a mean (e.g. a time mean) and primes denote departures from this mean. To the extent that the mean of the vertical velocity is small compared to the fluctuations about the mean, the skewness may be thought of as a measure of the up–down asymmetry of the vertical velocity distribution. The skewness of $-\omega$ is generally positive which implies stronger upward motions than downward motions.

The up–down asymmetry of vertical velocities has important implications for the distribution of precipitation and its extremes since precipitation is closely associated with upward motion (Sardeshmukh *et al.*, 2015; Pendergrass and Gerber, 2016). In addition, the up–down asymmetry of vertical velocities has an important influence on the moist effective static stability introduced by O'Gorman (2011). This effective static stability has been used to represent the effect of latent heating on the extratropical eddy length and eddy kinetic energy (O'Gorman, 2011), Hadley cell extent (O'Gorman, 2011; Levine and Schneider, 2015), deepening rates of cyclones (Booth *et al.*, 2015; Pfahl *et al.*, 2015), and Eliassen–Palm fluxes (Dwyer and O'Gorman, 2016). It is thus of interest to understand what controls the magnitude of the up–down asymmetry of the vertical velocity and how it may change as the climate warms.

Latent heating increases the asymmetry of the vertical velocity distribution because of its nonlinear relationship to vertical

motion: ascent often leads to condensation and latent heating whereas descent often does not lead to evaporation and negative latent heating because of an absence of condensate due to previous fallout of precipitation. Other diabatic effects such as cloud-radiative heating play a role in the dynamics of extratropical cyclones (e.g. Chagnon *et al.*, 2013) and could also affect the asymmetry of vertical velocities to the extent that they are related to vertical motion. The influence of latent heating on the asymmetry of vertical velocities was shown by Bjerknes (1938) for the case of moist convection. Recently, Pendergrass and Gerber (2016) developed a simple stochastic model based on the thermodynamic equation and used it to show how latent heating increases the skewness of the vertical velocity. The thermodynamic equation is a natural starting point for theories of the skewness because it includes both the latent heating term and a term involving the vertical velocity. However, the thermodynamic equation also includes terms such as horizontal advection of temperature whose statistical distribution must be assumed if the skewness of the vertical velocity is to be estimated.

For the Extratropics, the vertical velocity is better constrained by the combination of the vorticity and thermodynamic equations than by the thermodynamic equation alone. Many previous studies have investigated the idealized problem of small-amplitude moist baroclinic instability and found that latent heating reduces the relative area of updraughts to downdraughts, thus increasing the skewness of the vertical velocity by mass continuity, provided the nonlinearity associated with the absence of latent heating in descending regions is taken into account (e.g. Emanuel *et al.*, 1987; Fantini, 1990, 1995; Zurita-Gotor, 2005). Zurita-Gotor (2005) parametrized latent heating by multiplying the dry static stability by a factor r where there is ascent, and he then used a two-layer model to derive a 'bulk wavenumber law' for unstable modes which states that the ratio of updraught to downdraught wavenumbers is given by $r^{-1/2}$. Mass continuity implies that the ratio of updraught to downdraught vertical velocities should also scale as $r^{-1/2}$, which implies that the skewness of the vertical velocity should increase without bound as r decreases. In section 5 we make a simplified version of the theory of Pendergrass and Gerber (2016) based on the thermodynamic equation which also predicts that the skewness increases as r decreases.

The link between vertical velocity skewness and the parameter r may be used to reason about the effect of climate change on the skewness. Assuming ascending air is saturated, the parameter r is proportional to the ratio of the moist static stability, $-\partial\theta^*/\partial p$, to the dry static stability, $-\partial\theta/\partial p$, where θ is potential temperature and θ^* is saturated equivalent potential temperature*. O'Gorman (2011) found that, as the climate warmed from present-day values in an idealized GCM, the dry static static stability in the Extratropics increased and the stratification became close to moist adiabatic such that the moist static stability approached zero. This would imply r decreases with warming and the skewness of the vertical velocity should increase. (A similar argument has recently been used by Shi and Durran (2016) to explain decreases in the area of ascent associated with non-orographic precipitation extremes in response to climate warming in idealized GCM simulations.) Consistent in sign with this argument, Pendergrass and Gerber (2016) found that the skewness of the vertical velocity at 500 hPa increased in magnitude with climate warming in simulations from the Coupled Model Intercomparison Project phase 5 (CMIP5), although this was for a global rather than an extratropical average and there was a large range across models in

the rate of increase (from 0.57% K^{-1} to 22% K^{-1} for the RCP8.5 scenario).

A different measure of asymmetry enters the effective static stability for moist eddies as formulated in O'Gorman (2011). The effective static stability may be written as

$$-\left(\frac{\partial\theta}{\partial p}\right)_{\text{eff}} = -\frac{\partial\theta}{\partial p} + \lambda\left.\frac{\partial\theta}{\partial p}\right|_{\theta^*}, \qquad (2)$$

where $-\partial\theta/\partial p|_{\theta^*}$ is the dry static stability associated with a moist-adiabatic stratification, and λ is the asymmetry parameter. Note that in this article, we distinguish between the *reduced static stability* due to latent heating which applies only in saturated updraughts and the *effective static stability* defined above which, through λ, represents the overall effect of latent heating on eddies including updraughts and downdraughts. (The term effective static stability has previously been in some cases to refer to the reduced static stability in updraughts.) The asymmetry parameter λ is defined by

$$\lambda = \frac{\overline{\omega'\omega^{\uparrow\prime}}}{\overline{\omega'^2}}, \qquad (3)$$

where $\omega^{\uparrow} = \omega$ for upward motion and $\omega^{\uparrow} = 0$ otherwise. For zero mean vertical velocity, $\lambda = 0.5$ for vertical velocities that are symmetric between up and down, and $\lambda \to 1$ in the limit of vanishingly small updraught regions with infinitely fast updraughts. Compared to the skewness, λ is expected to be less sensitive to the fastest updraughts because the skewness involves a third power of ω, whereas λ involves only a second power. For cases with an isolated disturbance and zero-mean vertical velocity, λ may be a more robust metric because the skewness changes if zero values are added to the sample but λ does not.

O'Gorman (2011) found that the asymmetry parameter λ in the Extratropics also increased with warming over a wide range of climates simulated by an idealized GCM. However, the changes in λ were quite small, despite the moist static stability becoming small in warm climates. In addition, λ has been found to vary by only ~ 0.05 over the seasonal cycle in the Extratropics in reanalysis data (Mooring, 2011), despite large seasonal changes in temperature and latent heating. These results are seemingly inconsistent with the contraction in updraught area expected from moist baroclinic instability for small moist static stability, and they also seem inconsistent with the study of Booth *et al.* (2015) which shows that λ increases substantially as latent heating is increased in moist baroclinic life cycles. Thus, the asymmetry parameter λ seems to be less sensitive to warming than would be expected from moist baroclinic instability. We will show for the same idealized GCM as used in O'Gorman (2011) that the increases in extratropical skewness with warming are also much smaller than expected from moist baroclinic instability.

There are at least three possible explanations for the relatively weak increases in skewness or asymmetry parameter in response to warming in the idealized GCM simulations. The first and simplest explanation is that the GCM does not have adequate spatial resolution to resolve the narrow regions of ascent that would be needed to give a large skewness. A second possible explanation is that the representation of latent heating by a reduced static stability in previous studies of moist baroclinic instability, such as that of Zurita-Gotor (2005), is inadequate. For example, although the latent heating greatly reduces the moist static stability for updraughts in the lower and middle troposphere, there may still be regions of stronger moist static stability at upper levels which limit the effect of moisture on baroclinic instability, as discussed by Whitaker and Davis (1994). Alternatively, it may be necessary to have a representation of latent heating that includes the effects of moist convection rather than just saturated ascent. Indeed Fantini (1990) found that it was necessary to distinguish upright and slantwise convection when considering the limit of vanishing updraught area in the

---

*From Eq. (7) of Fantini (1995), we can write

$$r = \frac{\theta}{\theta^*}\frac{\Gamma_{\text{m}}}{\Gamma_{\text{d}}}\left(\frac{\partial\theta^*}{\partial p}\right)\Big/\left(\frac{\partial\theta}{\partial p}\right),$$

where Γ_{d} is the dry-adiabatic lapse rate and Γ_{m} is the moist-adiabatic lapse rate.

primitive equations. Lastly, a third possible explanation is that nonlinear equilibration to a state of macroturbulence reduces the skewness and asymmetry parameter λ from the values that would occur for small-amplitude moist baroclinic instability. (We use the term macroturbulence to refer to the turbulence of large-scale eddies in the troposphere following Held, 1999.) Indeed, the asymmetry parameter decreased in the decay stages of the moist baroclinic lifecycles of Booth *et al.* (2015). Here we investigate all three of these possible explanations using a variety of idealized GCM simulations that explore the influence of climate change, spatial resolution, representation of latent heating, and nonlinear equilibration on the up−down asymmetry of vertical motions in the extratropical troposphere.

As part of our investigation, we perform a series of simulations of moist baroclinic instability over a wide range of climates. Thus, we also address the question of how moist baroclinic instability changes as the climate warms, something that has not previously been addressed in the literature to our knowledge. Previous studies have shown that moisture can lead to a distinct type of baroclinic disturbance, known as a diabatic Rossby vortex or diabatic Rossby wave, for which diabatic potential vorticity generation is an essential dynamical process. Diabatic Rossby vortices or waves have been seen both in observations and in a range of different simulations (e.g. Raymond and Jiang, 1990; Snyder and Lindzen, 1991; Parker and Thorpe, 1995; Wernli *et al.*, 2002; Moore and Montgomery, 2004, 2005; Boettcher and Wernli, 2013). Here, we follow Moore and Montgomery (2004) in using the term diabatic Rossby vortex to refer to an isolated baroclinic disturbance for which diabatic potential vorticity (PV) generation is central to the dynamics, although it may have a propagation mechanism that is similar in some ways to that of Rossby waves (see discussion in Boettcher and Wernli, 2013). Remarkably, we find that, as the climate warms, the most unstable mode changes in character and transitions to an isolated diabatic Rossby vortex in sufficiently warm climates.

We begin by describing the idealized GCM and investigating the effect of climate warming and changes in spatial resolution on the skewness of the extratropical vertical velocities (and the asymmetry parameter) in fully nonlinear simulations (section 2). We then describe how the skewness varies with warming in simulations of moist baroclinic instability in the same GCM (section 3), and we discuss the diabatic Rossby vortex that occurs in warm climates (section 4). We further investigate the influence of nonlinear equilibration in some simplified simulations in which large-scale condensation and moist convection are replaced by a reduced static stability for updraughts (section 5). These simulations allow us to demonstrate that a smaller skewness can occur in fully nonlinear simulations as compared to unstable modes, even without a detailed representation of latent heating in the fully nonlinear simulations, and they also allow us to make simple comparisons with the results of Zurita-Gotor (2005) and Pendergrass and Gerber (2016). Lastly, we summarize our results and their implications (section 6).

2. Fully nonlinear simulations: impact of climate warming and resolution

We first consider fully nonlinear simulations run over a wide range of climates using an idealized aquaplanet GCM. The idealized GCM is not intended to realistically simulate all aspects of the general circulation, but rather it is useful as a model in which large changes in climate are readily simulated and the extent to which nonlinearity is included may be altered relatively easily. The GCM is based on a spectral version of the Geophysical Fluid Dynamics Laboratory (GFDL) atmospheric dynamical core, and it follows Frierson *et al.* (2006) and Frierson (2007) with details as in O'Gorman and Schneider (2008). The lower boundary condition is a thermodynamic mixed-layer ocean of depth 0.5 m with no horizontal heat transport or sea ice. Moist convection is parametrized using the scheme of Frierson (2007). Long-wave

radiation is treated using a two-stream grey scheme, and there are no seasonal or diurnal cycles of short-wave radiation. Cloud and water vapour radiative effects are not included in the model, but it would be interesting to study their possible influence on the skewness of the vertical velocity in future work. The default resolution is T85 in the horizontal with 30 vertical σ levels, where σ is pressure normalized by surface pressure. We also analyze T85 simulations with 20, 40, 60, and 90 vertical levels, and simulations with 30 vertical levels and horizontal spectral resolutions of T21, T42, T127, and T170. The T21 and T42 simulations with 30 levels are spun up over 800 days starting from an isothermal state. All other simulations are spun up over 300 days starting from the end state of another simulation.

The climate is varied in a series of simulations by altering a coefficient α that multiplies a fixed distribution of long-wave optical thickness in the radiation scheme. The resulting changes in long-wave optical thickness are a simple representation of changes in greenhouse gas concentrations. The values of α used are 0.4, 0.6, 0.7, 0.8, 0.9, 1.0, 1.2, 1.4, 1.6, 1.8, 2.0, 2.5, 3.0, 4.0, and 6.0. For each simulation, four-times daily output is collected over 300 days after spin-up. Statistics are averaged in time, zonally, and between the two hemispheres to take advantage of the interhemispheric and zonal symmetries of the insolation distribution and lower boundary. The global-mean surface air temperature T_g varies from 270 to 316 K for values of α from 0.4 to 6.0.

We will initially focus on a cold simulation ($\alpha = 0.4$ and $T_g = 270$ K), a reference simulation ($\alpha = 1.0$, $T_g = 288$ K) with a climate that is similar in some aspects to Earth's present-day climate, and a warm simulation ($\alpha = 4.0$, $T_g = 311$ K). The mean zonal winds and temperatures in each case are shown in Figure 1 of Pfahl *et al.* (2015). Representative snapshots of instantaneous mid-tropospheric vertical velocity at $\sigma = 0.48$ over the Northern Hemisphere are shown for these simulations in Figures 1(a), (c) and (e). It is evident from the snapshots that upward motions are stronger and cover less area than downward motions, at least for the reference and warm simulations. Plots of the same velocity field (at the same time) at a latitude of 44° are shown in Figures 2(a), (c) and (e).

For each simulation, the skewness and asymmetry parameter were calculated based on all ω between 40° and 60° latitude in both hemispheres at each time and level, and then averaged in time and vertically from the surface to the average tropopause level over the same latitude range. We focus on the 40° to 60° latitude range as representative of the Extratropics and to facilitate comparison with the simulations of moist baroclinic instability in the next section. The horizontal average used to calculate the skewness and the asymmetry parameter λ at each level and time was weighted by the surface pressure (because of the σ coordinate) and by the area of each gridbox. The tropopause was identified as the highest level at which the mean lapse rate is greater than $2 \, \mathrm{K \, km^{-1}}$.

The skewness of $-\omega$ increases with warming over most of the range of climates except for the warmest two climates (Figure 3(a)), and this implies stronger upward velocities relative to downward velocities as the atmosphere warms. The minimum and maximum values over the full range of climates are 1.3 and 2.2, respectively, and the overall increase in skewness is relatively modest given the large range of climates. The relatively small changes in skewness help explain why O'Gorman and Schneider (2009) were able to capture the leading-order changes in precipitation extremes in simulations with this idealized GCM using a physical scaling based on the root-mean-square vertical velocity; the changes in skewness may help to explain some of the deviations of the precipitation extremes from this scaling. The rate of increase of the skewness at the reference climate is $0.032 \, \mathrm{K^{-1}}$ relative to T_g, which corresponds to a fractional rate of increase of $2.0\% \, \mathrm{K^{-1}}$. To compare with the results for CMIP5 from Pendergrass and Gerber (2016), we also calculate the skewness at a fixed vertical level of $\sigma = 0.48$ which yields a higher rate of increase at the reference climate of $4.3\% \, \mathrm{K^{-1}}$
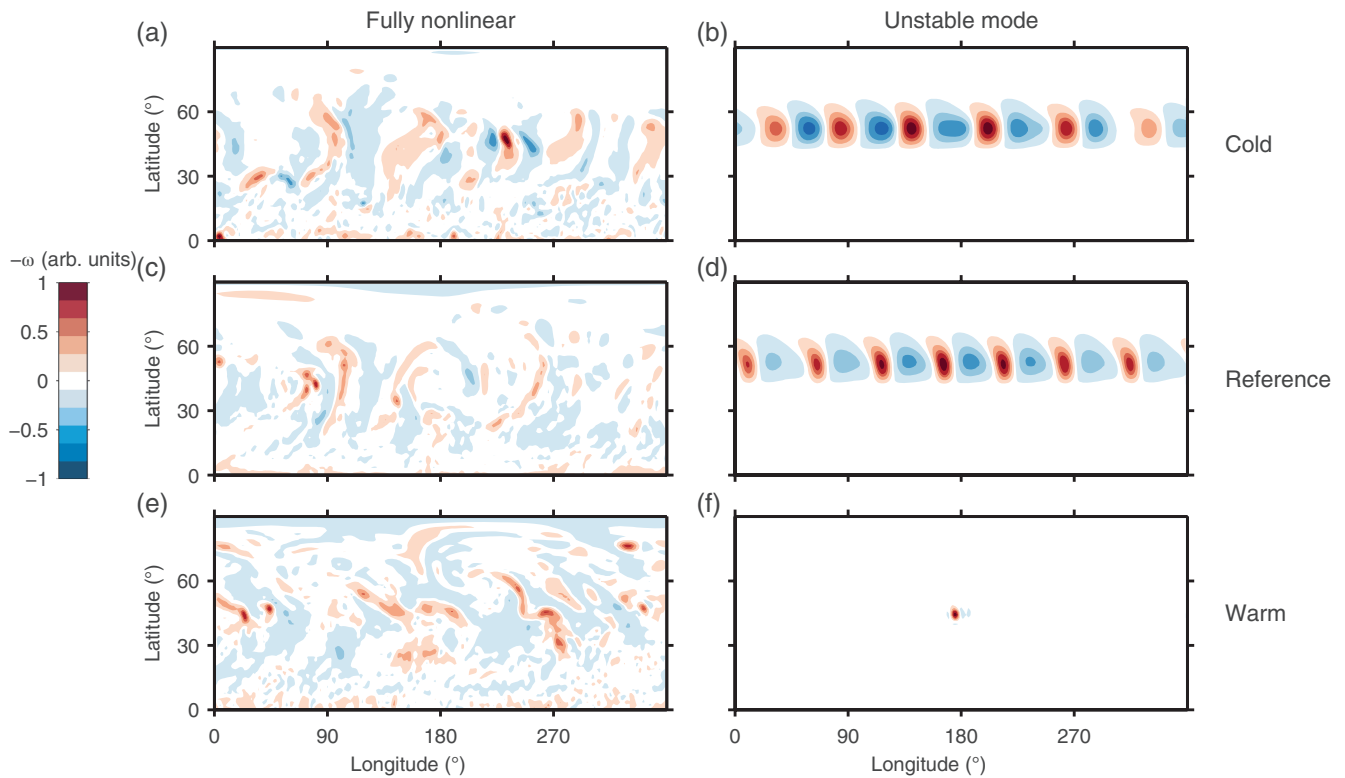
Figure 1. Snapshots of instantaneous vertical velocity ($-\omega$; red indicates upward motion) at a mid-tropospheric level ($\sigma = 0.48$) in simulations with the idealized GCM in (a, b) a cold climate ($T_g = 270$ K), (c, d) the reference climate ($T_g = 288$ K), and (e, f) a warm climate ($T_g = 311$ K). Snapshots are shown for fully nonlinear simulations in (a, c, e) and the most unstable modes of extratropical moist baroclinic instability in (b, d, f). Only the Northern Hemisphere is shown. In each panel, the vertical velocity is rescaled by its maximum absolute value for the purposes of presentation.
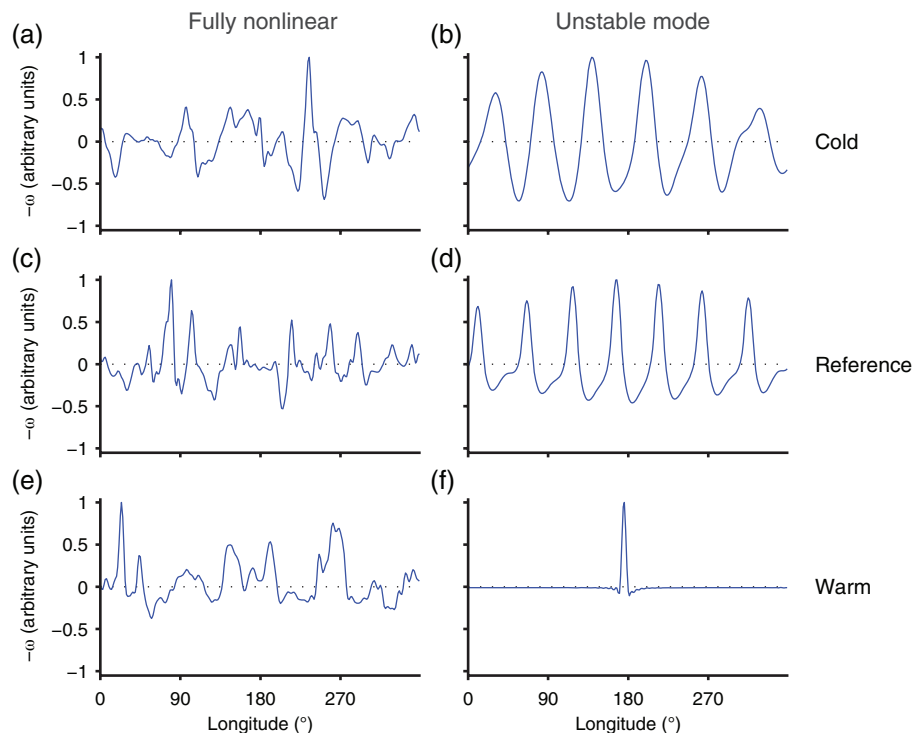

Figure 2. As Figure 1, but showing profiles of $-\omega$ at latitude 44°N. [Colour figure can be viewed at wileyonlinelibrary.com].

for the midlatitudes and 4.4% K^{-1} for the global skewness; these rates of change are in the range of $0.57-22\%$ K^{-1} across CMIP5 models which Pendergrass and Gerber (2016) found for the global skewness at 500 hPa.

The asymmetry parameter λ also increases with warming over most of the range of climates in a similar manner to the skewness (Figure 3(b)). The values of λ range from 0.65 to 0.72, and the rate of increase at the reference simulation is only 0.0025 K^{-1}, equivalent to a fractional rate of increase of 0.36% K^{-1}. In the effective static stability as defined in Eq. (2), λ is multiplied by the

dry static stability for a moist adiabatic stratification, $-\left.\partial\theta/\partial p\right|_{\theta*}$, which increases with warming at a fractional rate of 4% K^{-1} at 600 hPa and 0°C (Betts and Harshvardhan, 1987), and thus is considerably more sensitive to temperature than λ.

A possible explanation for the relative insensitivity of the skewness and λ to warming is that the GCM is unable to properly resolve narrow updraught regions in warm and moist climates. However, we find that λ only weakly depends on horizontal model resolution above T85 in the warm climate ($\alpha = 4.0$) as shown in Figure 4(b). This lack of sensitivity of λ to resolution
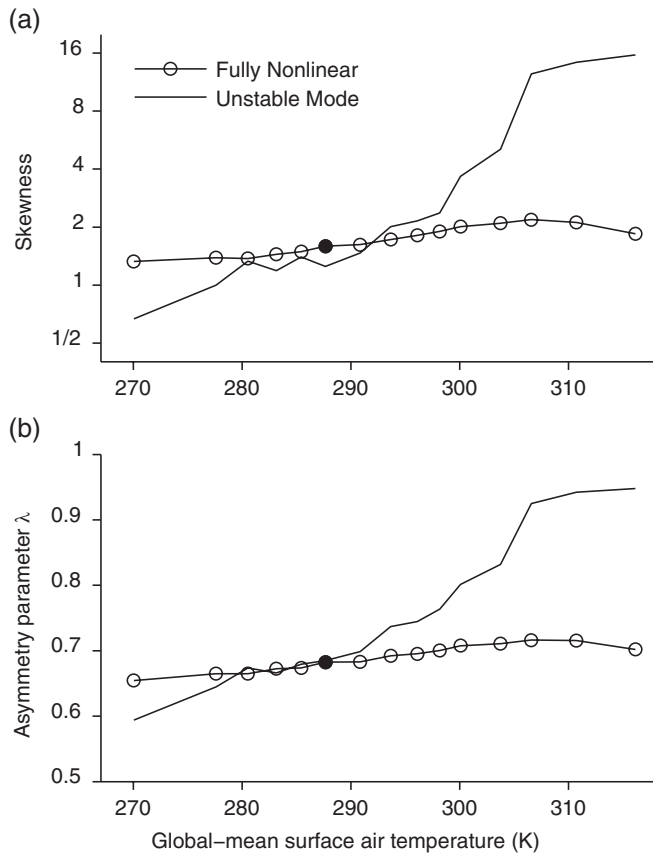
Figure 3. (a) The skewness of $-\omega$ and (b) the asymmetry parameter λ versus global-mean surface air temperature T_g (K) in simulations with an idealized GCM. Results are shown for fully nonlinear simulations (solid lines with circles) and for the most unstable modes of moist baroclinic instability (solid lines). The filled black circle indicates the reference simulation ($\alpha = 1$). The quantities shown are calculated for the midlatitude bands of 40–60° latitude in both hemispheres and then averaged in time and vertically over the troposphere. The unstable mode transitions from a quasi-periodic wave to an isolated vortex over the range 300–307 K.

is consistent with the results of Booth *et al.* (2015) for moist baroclinic lifecycles in which the vertical average of λ was found to be similar over a range of horizontal grid spacings from 3.125 to 200 km. Both λ and the skewness are found to be insensitive to vertical resolution in simulations with the number of vertical levels ranging from 20 to 90 and the default horizontal resolution of T85 (not shown). Unlike λ, the skewness continues to increase with increasing horizontal resolution from T127 to T170 (Figure 4(a)), and this increase does not seem to be due to sampling errors. Thus, we cannot argue that the skewness is fully converged with respect to horizontal resolution at T170. To confirm that horizontal resolution is not causing the weaker increase in skewness with warming compared to what is expected from moist baroclinic instability, we next turn to simulations of moist baroclinic instability with the idealized GCM at the same resolution as for the fully nonlinear simulations.

3. Moist baroclinic instability over a wide range of climates

Several studies of moist baroclinic instability have shown that the updraught area collapses as the moist static stability in the updraught region becomes small, implying a very skewed vertical velocity distribution. Here we investigate the behaviour of the skewness (and λ) for modes of moist baroclinic instability in the idealized GCM using the mean state from the fully nonlinear simulations as the basic state. This allows us to directly compare the skewness in the fully nonlinear simulations with the skewness for moist baroclinic instability at the same model resolution and with the same static stability distribution. Some previous idealized studies of moist baroclinic instability may have overestimated the role of moisture because they did not account for the vertical
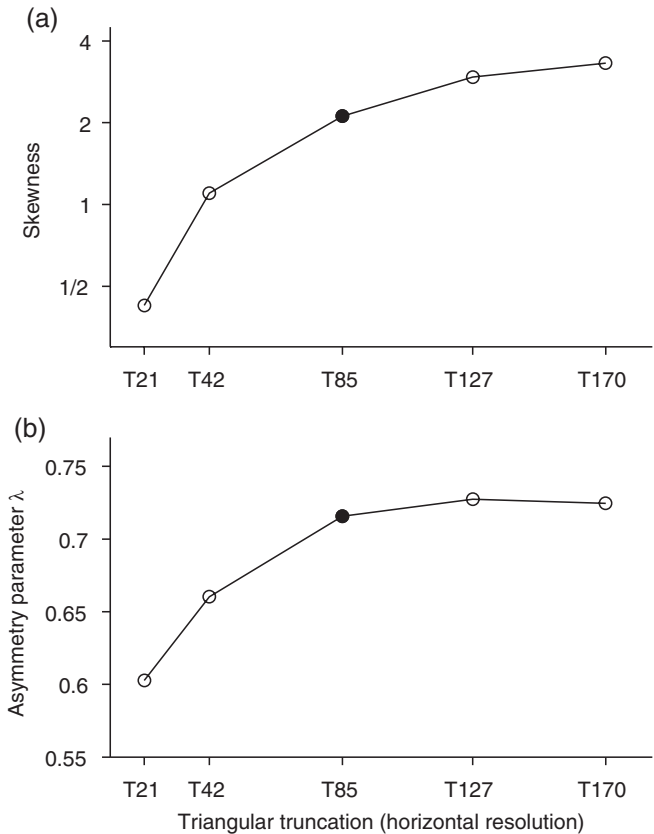

Figure 4. (a) The skewness of $-\omega$ and (b) the asymmetry parameter λ versus horizontal resolution in the fully nonlinear simulation with $\alpha = 4$. The filled black circle indicates the default resolution of T85. Results are shown for a warm climate ($\alpha = 4$), but the dependence on resolution is similar for the reference climate ($\alpha = 1$).

structure of the static stability; the moist static stability may not be small in the middle or upper troposphere, even when it is small in the lower troposphere (Whitaker and Davis, 1994). Here, we avoid this potential problem because our basic state includes the full structure of static stability from the fully nonlinear simulations. We also address the interesting question of how the nature of moist baroclinic instability changes as the climate warms.

The simulations of moist baroclinic instability isolate the fastest growing small-amplitude mode in the Extratropics using the zonal, time, and interhemispheric mean of the corresponding fully nonlinear simulation as the basic state. The meridional and vertical velocities of the basic state are set to zero. Boundary-layer drag has a strong effect on baroclinic instability (Valdes and Hoskins, 1988; Hall and Sardeshmukh, 1998), and we follow Merlis and Schneider (2009) in representing it by near-surface Rayleigh drag with a relaxation rate that decreases linearly in σ from a maximum value at the surface of $2 \, \text{day}^{-1}$ (a half-day time-scale) to zero for levels above $\sigma = 0.85$.

Periodic rescaling is used to maintain the eddies at small amplitude: when the eddy surface pressure reaches 1 Pa, the eddy components of all prognostic variables are rescaled to reduce their amplitude by a factor of 10 (e.g. Simmons and Hoskins, 1976; Merlis and Schneider, 2009). This rescaling removes advective nonlinear interactions between eddies in both the temperature and momentum equations. In addition, spectral coefficients with zonal wavenumber zero are not advanced in the time-stepping scheme in order to maintain the zonal-mean basic state. Thus, the simulations do not include the nonlinear influence of eddies on the zonal mean or advective nonlinear interactions between eddies. However, upward motion in the Extratropics is assumed to be saturated and to lead to large-scale condensation and latent heating, while downward motion is not associated with any latent heating, and thus the simulations are not linear.
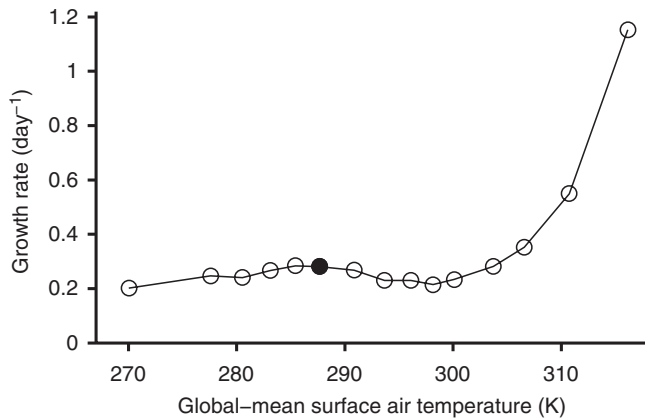
Figure 5. The growth rate (day^{-1}) of the most unstable mode versus global-mean surface air temperature T_g (K) in simulations with an idealized GCM. The filled black circle indicates the reference simulation ($\alpha = 1$). The unstable mode transitions from a quasi-periodic wave to an isolated vortex over the range 300–307 K.

The treatment of moisture is the key difference between dry linear baroclinic instability simulations with the primitive equations on the sphere (e.g. Simmons and Hoskins, 1976) and the moist baroclinic instability simulations that we present here. The GCM's large-scale condensation scheme is modified to maintain the atmosphere at saturation. In regions where the dynamics would lead to subsaturation, a positive specific humidity tendency is added to bring the specific humidity to saturation over the time step without an accompanying temperature tendency. In supersaturated regions, the large-scale condensation scheme is unmodified and there is a negative humidity tendency to reduce the humidity to saturation with a corresponding positive temperature tendency from latent heat release. Thus, the modified large-scale condensation scheme keeps the atmosphere saturated at all time steps and allows for latent heat release where there is upward motion. The moist convection scheme, radiation scheme, boundary-layer scheme, and surface fluxes are all deactivated. With large-scale condensation at all latitudes, the fastest-growing waves were found to occur in the Tropics and low latitudes. To focus on the extratropical instability, we do not allow large-scale condensation to act equatorward of 40° latitude. Furthermore, we impose additional Rayleigh drag with a rate of 40 day^{-1} (a time-scale of about a half hour) throughout the atmosphere equatorward of 40° latitude. This additional drag prevents the wave from penetrating equatorward into the dry region, which would make it a mixed moist and dry wave and thus more difficult to interpret.

A weak perturbation is added to the initial condition's vorticity in zonal wavenumbers 5 and 6 over all model levels to seed the eddy field. Instantaneous fields are stored once per day and the simulations are run for 300 days. The final rescaling of amplitude is performed at a set time (day 290) to facilitate calculation of growth rates. The growth rates are calculated using the rate of change of the eddy meridional velocity evaluated poleward of 40° latitude at $\sigma = 0.84$ over days 291 to 294.

Snapshots of $-\omega$ at $\sigma = 0.48$ are shown at day 292 of the moist baroclinic instability simulations in Figures 1(b),(d) and (f) and 2(b),(d) and (f). The snapshots show a marked change in the structure of ω as the climate warms. In the cold simulation, the most unstable mode is a quasi-periodic wave with zonal wavenumber 6 that is fairly symmetric between up and down. In the reference simulation, the most unstable mode is also wave-like with zonal wavenumber 7, but it exhibits an updraught region that is markedly more narrow than the downdraught region. For the warm simulation, the most unstable mode is not wave-like, but instead it exhibits the structure of a diabatic Rossby vortex with a single narrow updraught surrounded by widespread weak subsidence. Inspection of snapshots suggests that the break-up of the periodic wave begins in the $\alpha = 2$, $T_g = 300$ K

simulation, and only a single isolated vortex remains in the $\alpha = 3$, $T_g = 307$ K simulation (the corresponding midlatitude surface air temperatures averaged over 40–60° latitude are 292 K for $\alpha = 2$ and 299 K for $\alpha = 3$). The emergence of this different type of moist instability leads to an increase in the growth rates of the modes in the warmest climates (Figure 5). The physical reason for the change in the nature of the instability from wave-like to isolated vortex is the increased dynamical importance of latent heating. Latent heating occurs in updraughts but not in downdraughts and thus breaks the symmetry of the wave, as discussed in more detail in the next section.

The snapshots of $-\omega$ for the unstable modes in Figures 1(b), (d) and (f) show a striking increase in the up–down asymmetry of vertical motion in the unstable modes as the climate warms. Figure 3 confirms that there is a general increase with warming in both the skewness of $-\omega$ and in the asymmetry parameter for the unstable modes. (The skewness and asymmetry parameter are calculated as for the fully nonlinear simulations and averaged in time over days 291–294.) However, the unstable modes greatly overestimate the increase in skewness with warming compared to the fully nonlinear simulations (Figure 3(a)). The skewness ranges from 0.67 to 15.7 for the unstable modes compared to 1.3 to 2.2 for the fully nonlinear simulations. The dependence of skewness on temperature is not smooth for the unstable modes, which makes it difficult to estimate a rate of increase with respect to temperature at the reference simulation ($\alpha = 1$). Linear regression of skewness against T_g over the seven simulations from $\alpha = 0.7$ to 1.6 gives a rate of increase of 0.058 K^{-1} for the unstable modes which is roughly double the corresponding value of 0.028 K^{-1} for the fully nonlinear simulations. For the unstable modes, the break-up of the wave into a vortex from $T_g = 300 - 307$ K is marked by a particularly sharp increase in skewness. The asymmetry parameter λ for the unstable modes exhibits an evolution with temperature that is qualitatively similar to that of the skewness (Figure 3(b)), which suggests that this behaviour is robust to changes in how the up–down asymmetry is measured.

For the coldest two simulations, the skewness is smaller for the unstable modes than for the fully nonlinear simulations. The coldest simulations have low specific humidities, and so we are motivated to ask: what could cause asymmetry in the vertical velocity in the dry limit? The finite amplitude wave in the dry inviscid semi-gesotrophic Eady model shown in Figure 6 of Emanuel et al. (1987) does not exhibit an asymmetry between upward and downward motion. However, the vertical velocity distribution is asymmetric in the dry baroclinic lifecycle shown in Figure 2(a) of Booth et al. (2015), and the asymmetry is largest in the lower troposphere. One possible contributor to this dry asymmetry in vertical velocity is an asymmetry in Ekman pumping at the surface driven by the greater pressure gradients in cyclones than anticyclones. This asymmetry between cyclones and anticyclones is found to increase with Rossby number according to the QG+1 equations of Rotunno et al. (2000); that we should expect greater asymmetry between cyclones and anticyclones at higher Rossby number also follows more simply from gradient wind balance (e.g. Martin, 2006). Our fully nonlinear simulations have higher Rossby number than the small-amplitude unstable modes, and this may explain why they have more skewed vertical velocities in cold and dry climates. The difference in Rossby numbers is also present in the warm climates, but these climates have the additional factor of strong latent heating which strongly increases the skewness for the unstable modes.

We explored the robustness of the behaviour of the unstable modes by running an alternative series of instability simulations without the additional Rayleigh drag equatorward of 40° latitude, and a second alternative series in which the radiation scheme was not turned off. Although there are some differences in details, the main results that there is a strong increase in skewness with warming and that the unstable mode switches from periodic
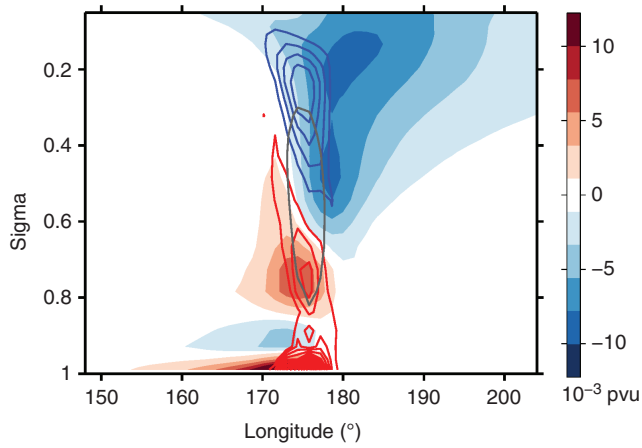
Figure 6. Structure of the most unstable mode in a warm climate ($\alpha = 4.0$; $T_g = 311$ K), showing the potential vorticity (PV) anomalies with respect to the zonal mean (red and blue shading) and the diabatic generation rate of PV by large-scale condensation (positive (red) and negative (blue) contours with interval 4×10^{-8} pvu s^{-1}; the zero contour is not plotted). The grey contour is one value (2.5×10^{-6} K s^{-1}) of the potential temperature tendency from large-scale condensation. The fields are plotted at 44°N versus longitude and σ at the same time as in Figures 1(f) and 2(f). The PV used is the hydrostatic approximation to Ertel's PV. Note that the overall amplitude of the fields is arbitrary.

waves to isolated vortices in warm climates are unaffected by these changes[†]

The result that the unstable modes can achieve very high values of the skewness of the vertical velocity suggests that the limited resolution of the idealized GCM is not responsible for the relatively weak increases in skewness with warming in the fully nonlinear simulations. Also, the fact that the unstable modes are calculated using the mean state from the fully nonlinear simulations implies that we cannot explain the relatively low skewness of the fully nonlinear simulations in warm climates by the vertical structure of the moist static stability (cf. Whitaker and Davis, 1994).

4. Diabatic Rossby vortices in warm climates

The change in the most unstable mode from a quasi-periodic wave to an isolated vortex as the climate warms (compare Figures 1(d) and (f)) is a striking indicator that latent heating is playing a key role in the dynamics of the modes in the warm climates. The PV anomalies of the most unstable mode in the warm simulation ($\alpha = 4.0$; $T_g = 311$ K) are shown in Figure 6. There is an anticyclonic PV anomaly in the upper troposphere, and a cyclonic PV anomaly located slightly westward in the lower troposphere. We will focus on the anomalies in the free troposphere, but there are also PV anomalies of both signs in the boundary layer. The meridional velocity is poleward on the western flank of the upper-tropospheric PV anomaly and on the eastern flank of the lower-tropospheric PV anomaly, and thus the meridional velocity tilts westward with height (not shown). Because temperature decreases poleward in the basic state, there is ascending air on the western side of the upper-tropospheric PV anomaly and descending air on the eastern side (and these induced velocities extend vertically beyond the PV anomaly). However, the fact that latent heating is only associated with upward motion and not downward motion implies that latent heating only occurs on the western side of the upper-tropospheric PV anomaly but not on the eastern side (see grey contour in Figure 6). Similarly there

is latent heating on the eastern side of the lower-tropospheric PV anomaly, but not on the western side. Thus, to the extent that latent heating is central to the dynamics of the unstable mode, it cannot take the form of a periodic wave in longitude but instead must be an isolated vortex, as discussed by Parker and Thorpe (1995).

Figure 6 also shows the diabatic generation rate of PV by large-scale condensation. As expected, the diabatic generation of PV from latent heating takes the form of a vertical dipole centred at the longitude (176°) of maximum upward motion, with negative generation in the upper troposphere above the level of maximum latent heating and positive generation in the lower troposphere below the level of maximum latent heating. The configuration of the PV anomalies and diabatic PV generation is such that the generation tends to amplify the PV anomalies while also helping the upper and lower anomalies to phase lock despite advection by the westerly vertical shear. A mode of this type in which diabatic PV generation and interior PV anomalies are key was first discussed by Snyder and Lindzen (1991), although they allowed for negative latent heating in descent regions and thus obtained a periodic wave rather than an isolated vortex. The interaction between the upper and lower PV anomalies is necessary for growth and is consistent with the interpretation of instability through counterpropagating Rossby waves as applied to a moist atmosphere (De Vries *et al.*, 2010). For simplicity, we refer to the whole structure as a diabatic Rossby vortex[‡].

Our unstable mode is similar to the diabatic Rossby vortex found in an initial-value problem by Moore and Montgomery (2005), taking into account the warmer climate, higher tropopause and saturated ascent being considered here. A transition from waves to a vortex-dominated regime with increased latent heating was also found by Lapeyre and Held (2004) in a moist quasi-geostrophic two-layer model, although in that model the dynamics were nonlinear and the vortices had cyclonic vorticity in both the lower and upper layers.

It is a remarkable result of our analysis of the idealized GCM simulations that the most unstable mode switches to a diabatic Rossby vortex in sufficiently warm and moist climates. This raises the question of whether there is a corresponding transition in the prevalence of diabatic Rossby vortices in the fully nonlinear simulations. Pfahl *et al.* (2015) tracked extratropical cyclones in the fully nonlinear simulations and found that the maximum deepening rates along the cyclone tracks decreased with warming for sufficiently warm climates, unlike what is found for the growth rates of the unstable modes (Figure 5). However, Pfahl *et al.* (2015) found that the behaviour of the deepening rates varied depending on whether median or high percentiles were considered, and the dynamics of the diabatic Rossby vortices could still be relevant for certain classes of fast-growing disturbances in the fully nonlinear simulations. In future work, it would be interesting to extend previous compositing studies for this idealized GCM (Pfahl *et al.*, 2015; Tamarin and Kaspi, 2016) by compositing the PV structure and diabatic PV generation rate for cyclones in their growth phase in different climates and comparing the composites with the most unstable modes. It would also be interesting to investigate whether there is a change in the prevalence of diabatic Rossby vortices with warming in more comprehensive models that include processes such as cloud-radiative effects.

5. Simulations with reduced static stability for updraughts

The results so far suggest that the skewness of the vertical velocity behaves differently for the modes of moist baroclinic instability than in the fully nonlinear simulations. One plausible reason

---

[†]Without the additional Rayleigh drag, the growth rates of the unstable modes are higher, there are two or three diabatic Rossby vortices in the warmest simulations rather than one, and there is a higher zonal wavenumber and a lower skewness in the colder simulations. Also, there is ringing in the instantaneous fields that presumably results from the sharp transition in latent heating at 40° latitude and which is not found to occur when the additional drag is imposed. With the radiation scheme kept on, the growth rates of the unstable modes are lower in most of the climates.

[‡]Note that De Vries *et al.* (2010) and Cohen and Boos (2016) have used a different dynamical nomenclature in which diabatic Rossby waves are classified as involving an interaction between surface baroclinicity and an interior PV anomaly rather than between two interior PV anomalies as seems to occur in Figure 6. We note that there could also be a contribution to the dynamics from the surface air temperature anomalies in our unstable mode.

for this is that advective nonlinear eddy–eddy interactions lead to different balances in the thermodynamic equation than occur in the (small-amplitude) unstable mode regime. In addition, nonlinear equilibration to macroturbulence leads to the presence of disturbances that differ from the unstable mode (i.e. disturbances that are experiencing non-modal growth or decaying). However, our simulations of moist baroclinic instability also differ from the fully nonlinear simulations by assuming that upward motion is saturated and by only including latent heating from large-scale condensation and not from the moist convection scheme.

To further investigate the cause of the different behaviour of the skewness in the fully nonlinear simulations and simulations of moist baroclinic instability, we next investigate a series of simulations in which the large-scale condensation and moist convection schemes are turned off. The default resolution (T85 and 30 vertical levels) and reference value of the long-wave absorber parameter ($\alpha = 1$) are used. In the place of the moist parametrizations, latent heating is represented more simply by a reduction in the dry static stability whenever there is upward motion in the troposphere. The thermodynamic equation in the idealized GCM is modified so that the dry static stability is multiplied by a prescribed factor r whenever there is upward motion below roughly 200 hPa, and this factor r is varied over a range of values from 0.01 to 1 in a series of simulations ($r = 1$ corresponds to no reduction in static stability). More specifically, a factor $\mathcal{R}(p, \omega)$ is introduced into the thermodynamic equation

$$\frac{\partial \theta}{\partial t} = \ldots - \omega \frac{\partial \theta}{\partial p} \mathcal{R}(p, \omega).$$

The factor $\mathcal{R}(p, \omega)$ is set to 1 for $\omega \geq 0$ and to

$$r + 0.5(1 - r)\left\{1 - \tanh\left(\frac{p - p_u}{p_w}\right)\right\} \quad \text{for} \quad \omega < 0,$$

where $p_u = 200$ hPa is the nominal uppermost pressure level for the reduction in static stability, and $p_w = 50$ hPa is the width of the transition region about this level. This approach is similar in spirit to the simplified representations of latent heating or convection considered in past studies of moist baroclinic instability (e.g. Emanuel *et al.*, 1987; Zurita-Gotor, 2005) and it allows us to make a stronger connection with the results of those studies. However, here we apply this reduced static stability formulation in a GCM and we apply it to both simulations of small-amplitude moist baroclinic instability and to simulations in which the flow undergoes nonlinear equilibration to a macroturbulent state.

The simulations are started with a small-amplitude perturbation to the mean state of the reference simulation (from section 2), and the disturbance is allowed to grow to finite amplitude, non-linearly equilibrate, and develop into full macroturbulence. To avoid large changes in the mean state due to the strong diabatic heating implied by the smaller values of the static stability reduction factor r, the zonal means of temperature, zonal wind and surface pressure are strongly relaxed to the zonal and time-mean state of the reference simulation, and the zonal-mean meridional wind is relaxed to zero. The relaxation time-scale for all variables is 4 h. Using a short relaxation time rather than simply fixing the zonal mean state was found to improve numerical stability, and the small-scale filter used in the model was also increased in strength to further improve numerical stability. Since the mean state is not allowed to fully adjust in these simulations, they are not fully nonlinear, and so we refer to their statistical equilibrium state as macroturbulence to emphasize the presence of advective nonlinear eddy–eddy interactions and multiple growing and decaying disturbances.

The most unstable mode was also calculated for each value of r following the small-amplitude approach described in section 3 and using the zonal and time mean of the reference simulation as the basic state (but with the mean meridional and vertical wind
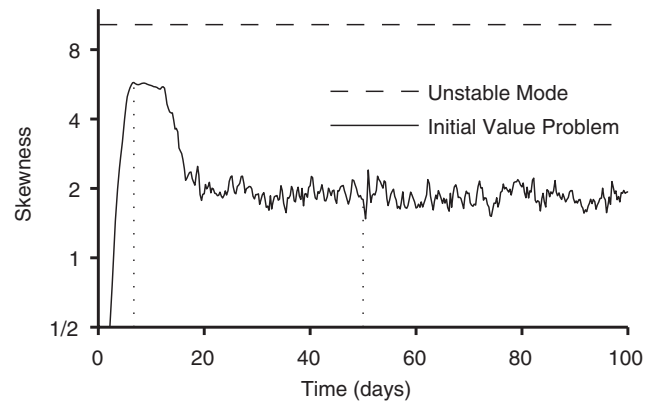

Figure 7. The skewness of $-\omega$ as a function of time in the first 100 days of a simulation in which the static stability for updraughts is multiplied by a factor of $r = 0.01$ (solid line). The skewness is calculated at each level and time based on all ω values between 25° and 65° latitude in both hemispheres, and then it is averaged vertically over the troposphere. The value for the most unstable mode, calculated using the periodic rescaling approach, is shown for comparison (horizontal dashed line). The two times in Figure 8 are shown as vertical dotted lines.
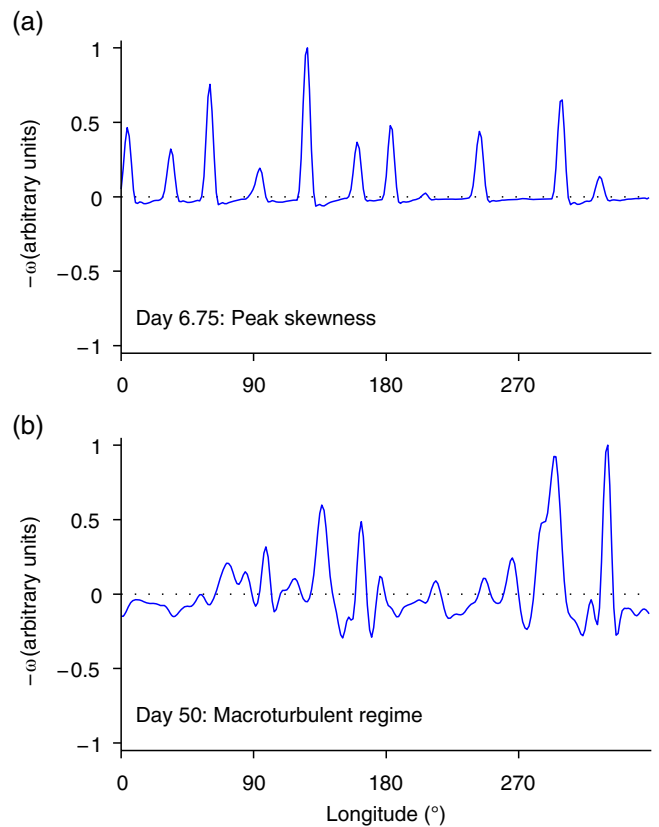

Figure 8. Example snapshots of $-\omega$ (with positive values denoting upward motion) at $\sigma = 0.48$ versus longitude for the simulation shown in Figure 7 in which the static stability for updraughts is multiplied by a factor of $r = 0.01$: (a) day 6.75 and latitude 29°N at the time of peak skewness, and (b) day 50 and latitude 50°N during the statistical equilibrium period when the macroturbulence is established. Note that for small values of r, the storm track in the macroturbulent state tends to occur further poleward than the initial instability. [Colour figure can be viewed at wileyonlinelibrary.com].

set to zero). Unlike in section 3, it was not necessary to impose additional drag at low latitudes since waves in the Tropics are not unstable in this set-up. The most unstable mode was determined from a 200-day integration.

5.1. Reduction of skewness and asymmetry parameter by nonlinear equilibration

The skewness of $-\omega$ was first calculated at each level and time based on values between 25° and 65° latitude in both hemispheres, and then averaged vertically from the surface to the mean level of
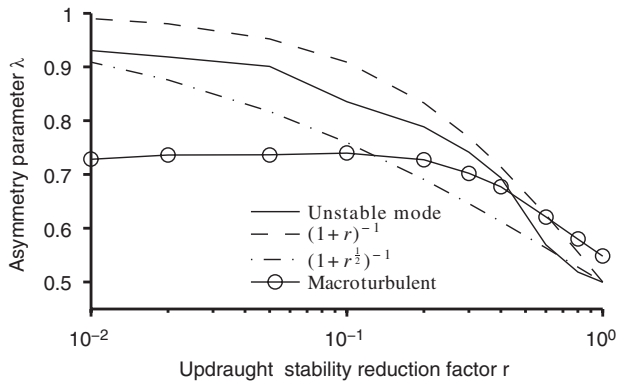
Figure 9. Asymmetry parameter λ versus the updraught static-stability reduction factor *r* for the unstable modes (solid line) and the macroturbulent state (solid line with circles). Also shown for comparison are theoretical estimates based on the thermodynamic equation (dashed line) and the 'bulk wavenumber law' of Zurita-Gotor (2005) for unstable modes (dash-dotted line).

the tropopause over this latitude range. A wider latitude band than in previous sections is needed here because the unstable modes are not necessarily localized in the $40-60°$ latitude band. Figure 7 shows the skewness as a function of time in the simulation with $r = 0.01$, as well as the value for the corresponding unstable mode. The skewness grows rapidly at first, but nonlinear equilibration causes it to plateau at a value somewhat lower than that of the unstable mode and then reduce to a value more typical of the fully nonlinear simulations discussed in section 2. Example $-\omega$ profiles versus longitude are shown for the time of the peak skewness in Figure 8(a) and for a time during the macroturbulent regime in Figure 8(b), and these profiles clearly show the striking reduction of the asymmetry between updraughts and downdraughts with nonlinear equilibration.

To illustrate the behaviour for a range of different values of *r*, the asymmetry parameter λ was calculated at each time in the same way as for the skewness discussed above, and then averaged in time over 5 days (days 191–194) for the unstable mode simulation based on once-daily data, and over 100 days (days 101–200) in the macroturbulent state based on four-times daily data. Figure 9 shows that λ for the unstable modes grows monotonically as *r* is decreased, whereas λ for the macroturbulent state grows at first as *r* is decreased but then remains roughly constant at a value slightly greater than 0.7 for $r < 0.2$.

The implication of these results for the simulations with more realistic latent heating discussed in sections 2 and 3 is that nonlinear equilibration is sufficient to explain much of the difference in skewness and λ between the unstable modes and the fully nonlinear simulations in warm climates. We cannot rule out that differences in how latent heating is represented for the unstable modes versus fully nonlinear simulations also make some contribution.

5.2. Evaluation of theories for the asymmetry parameter

The unstable modes may still be relevant for the growth phase of particular disturbances, and previous work has shown that the effective static stability may be used to estimate the effect of latent heating on the growth rate of cyclones in moist baroclinic lifecycles (Booth *et al.*, 2015). It is therefore of interest to evaluate whether the asymmetry parameter λ of the unstable modes as a function of *r* may be estimated from the theories of Zurita-Gotor (2005) and Pendergrass and Gerber (2016). To make the simplest comparison with theory, we consider a piecewise constant profile of ω (with single values for the updraught and downdraught regions) and with zero mean. O'Gorman (2011) showed that in this case $\lambda = 1 - a_u$, where a_u is the updraught area fraction given by $L_u/(L_u + L_d)$ with L_u and L_d the horizontal length-scales of the updraught and the downdraught, respectively. We represent latent heating by multiplying the dry static stability $-\partial\theta/\partial p$ by a factor *r* when there is upward motion.

As discussed in the introduction, the 'bulk wavenumber law' of Zurita-Gotor (2005) for unstable modes implies that $L_u/L_d = r^{1/2}$ and thus $\lambda = (1 + r^{1/2})^{-1}$, which gives some sense of the increase in λ of the unstable modes as *r* decreases (Figure 9), although it tends to underestimate λ in most cases. A more detailed calculation (not shown) based on choosing representative analytical ω profiles for updraught and downdraught regions and applying the matching condition between updraught and downdraught regions given in the appendix of Zurita-Gotor (2005) reveals that the value of λ depends on how the updraughts and downdraughts are arranged, and that higher values of λ result when an isolated updraught is surrounded by two downdraughts that decay exponentially away from the updraught rather than having a periodic wave. This helps to explain the underestimate of λ by $(1 + r^{1/2})^{-1}$ at low *r* in Figure 9, since the periodic wave tends to break up into isolated vortices as *r* is decreased.

We can also simplify the model of Pendergrass and Gerber (2016) based on the thermodynamic equation to give an estimate of λ for the piecewise-constant profile of ω and the reduced-static-stability representation of latent heating. Following Pendergrass and Gerber (2016), we denote by Q_n the sum of the terms in the thermodynamic equation other than the latent heating term and the term involving the vertical velocity. For upward motion, $\omega r\partial\theta/\partial p = Q_n$, whereas for downward motion, there is no latent heating and $\omega\partial\theta/\partial p = Q_n$. Further assuming that Q_n has the same magnitude (but opposite sign) for updraughts and downdraughts, the ratio of updraught velocity to downdraught velocity scales as r^{-1}. Mass continuity then gives that $L_u/L_d = r$ and $\lambda = (1 + r)^{-1}$, which also gives some sense of the increase in λ with decreasing *r* for the unstable modes (Figure 9). This simple prediction for λ is not affected by changes in the magnitude of Q_n, but it would be altered if the assumption that Q_n has the same magnitude for upward and downward motions were relaxed. (Pendergrass and Gerber, 2016, give a more general analysis of the effects of changes in the distribution of Q_n.)

Both theoretical arguments discussed in this section suggest that λ approaches 1 for small *r*, broadly consistent with the behaviour of the unstable modes. However, for the macroturbulent state, λ clearly saturates at a value much smaller than 1 for $r < 0.2$. This is the relevant limit of *r* when the moist static stability is small (as expected in sufficiently warm climates as discussed in O'Gorman, 2011), and thus it is desirable to develop a theory for the asymptotic value of λ or skewness that is reached in the macroturbulent regime.

6. Conclusions

We have examined the skewness of the extratropical vertical velocity distribution in different climates using a series of idealized GCM simulations. The skewness increases with warming over most of the range of climates considered. However, the skewness does not increase with warming to the same extent as would be expected from moist baroclinic instability, and this is also the case for the asymmetry parameter that appears in the effective static stability of O'Gorman (2011). Our results suggest that this relative insensitivity is not an artifact of limited spatial resolution in the idealized GCM or the simplified representation of latent heating used in some previous studies of moist baroclinic instability. Instead the difference in behaviour between the fully nonlinear simulations and the simulations of moist baroclinic instability arises because nonlinear equilibration to a macroturbulent state can greatly reduce the skewness in warm climates. While previous studies (Emanuel *et al.*, 1987; Zurita-Gotor, 2005) provide theoretical guidance as to the area fraction of ascent of unstable modes of moist baroclinic instability, and this can be used to predict the skewness or asymmetry parameter for these modes, further work is needed to develop a theory for the quite different behaviour that occurs in warm climates when the instability is allowed to equilibrate and the flow becomes fully nonlinear. Our simplified version of the theory of Pendergrass and Gerber (2016) based

on the thermodynamic equation behaves more similarly to the unstable modes than the fully nonlinear simulations in the limit of small moist static stability that is relevant for warm climates.

Future work could also investigate the extent to which changes in the extratropical skewness or asymmetry parameter in response to climate change are robust across different comprehensive GCMs and whether they depend on the choice of convection schemes or other parametrizations. Changes in the skewness of the vertical velocity are expected to be linked to changes in the intensity and spatial extent of precipitation events. Changes in the intensity distribution of precipitation are more robust across models for the Extratropics than for the Tropics (O'Gorman and Schneider, 2009; Pendergrass and Hartmann, 2014), while changes in the spatial extent of midlatitude precipitation extremes in CMIP5 simulations are relatively small in magnitude (Dwyer and O'Gorman, 2017), which suggests that changes in the skewness of the vertical velocity may be smaller and more robust across models in the Extratropics than the Tropics. It would also be useful to study the skewness of the vertical velocity separately over mountainous regions since Shi and Durran (2016) found that the contribution of changes in vertical velocity to changes in precipitation extremes in idealized GCM simulations was positive over oceans and plains but mostly negative over mountainous regions.

We have shown that the vertical velocity distribution in unstable modes behaves differently from the overall vertical velocity distribution in fully nonlinear macroturbulence, but the unstable modes may still be relevant to particular fast-growing disturbances. An interesting result of our analysis is that the most unstable mode transitions from a quasi-periodic wave to an isolated diabatic Rossby vortex in sufficiently warm and moist climates. The break-up of the periodic wave in our idealized GCM simulations begins at a midlatitude surface air temperature of 292 K which is not far from the Earth's summer temperatures in northern midlatitudes. Therefore, it would be interesting to investigate in future work whether the transition of the most unstable mode to diabatic Rossby vortices occurs for a basic state taken seasonally from different climates simulated by comprehensive GCMs. It would also be of interest to track diabatic Rossby vortices in fully nonlinear simulations and investigate their behaviour as the climate warms.

Acknowledgements

References

Betts AK, Harshvardhan. 1987. Thermodynamic constraint on the cloud liquid water feedback in climate models. *J. Geophys. Res.* **92**: 8483–8485. https://doi.org/10.1029/JD092iD07p08483.

Bjerknes J. 1938. Saturated-adiabatic ascent of air through dry-adiabatically descending environment. *Q. J. R. Meteorol. Soc.* **64**: 325–330.

Boettcher M, Wernli H. 2013. A 10-yr climatology of diabatic Rossby waves in the Northern Hemisphere. *Mon. Weather. Rev.* **141**: 1139–1154.

Booth JF, Polvani L, O'Gorman PA, Wang S. 2015. Effective stability in a moist baroclinic wave. *Atmos. Sci. Lett.* **16**: 56–62.

Chagnon JM, Gray SL, Methven J. 2013. Diabatic processes modifying potential vorticity in a North Atlantic cyclone. *Q. J. R. Meteorol. Soc.* **139**: 1270–1282.

Cohen NY, Boos WR. 2016. Perspectives on moist baroclinic instability: Implications for the growth of monsoon depressions. *J. Atmos. Sci.* **73**: 1767–1788.

De Vries H, Methven J, Frame TH, Hoskins BJ. 2010. Baroclinic waves with parameterized effects of moisture interpreted using Rossby wave components. *J. Atmos. Sci.* **67**: 2766–2784.

Dwyer JG, O'Gorman PA. 2016. Moist formulations of the Eliassen-Palm flux and their connection to the surface westerlies. *J. Atmos. Sci.* **74**: 513–530.

Dwyer JG, O'Gorman PA. 2017. Changing duration and spatial extent of midlatitude precipitation extremes across different climates. *Geophys. Res. Lett.* **44**: 5863–5871. https://doi.org/10.1002/2017GL072855.

Emanuel KA, Fantini M, Thorpe AJ. 1987. Baroclinic instability in an environment of small stability to slantwise moist convection. Part I: Two-dimensional models. *J. Atmos. Sci.* **44**: 1559–1573.

Fantini M. 1990. Nongeostrophic corrections to the eigensolutions of a moist baroclinic instability problem. *J. Atmos. Sci.* **47**: 1277–1287.

Fantini M. 1995. Moist Eady waves in a quasigeostrophic three-dimensional model. *J. Atmos. Sci.* **52**: 2473–2485.

Frierson DMW. 2007. The dynamics of idealized convection schemes and their effect on the zonally averaged tropical circulation. *J. Atmos. Sci.* **64**: 1959–1976.

Frierson DMW, Held IM, Zurita-Gotor P. 2006. A gray-radiation aquaplanet moist GCM. Part I: Static stability and eddy scale. *J. Atmos. Sci.* **63**: 2548–2566.

Hall NMJ, Sardeshmukh PD. 1998. Is the time-mean Northern Hemisphere flow baroclinically unstable? *J. Atmos. Sci.* **55**: 41–56.

Held IM. 1999. The macroturbulence of the troposphere. *Tellus A-B* **51**: 59–70.

Lapeyre G, Held IM. 2004. The role of moisture in the dynamics and energetics of turbulent baroclinic eddies. *J. Atmos. Sci.* **61**: 1693–1710.

Levine XJ, Schneider T. 2015. Baroclinic eddies and the extent of the Hadley circulation: An idealized GCM study. *J. Atmos. Sci.* **72**: 2744–2761.

Martin JE. 2006. *Mid-latitude Atmospheric Dynamics: A First Course.* John Wiley & Sons: Chichester, UK.

Merlis TM, Schneider T. 2009. Scales of linear baroclinic instability and macroturbulence in dry atmospheres. *J. Atmos. Sci.* **66**: 1821–1833.

Moeng CH, Rotunno R. 1990. Vertical-velocity skewness in the buoyancy-driven boundary layer. *J. Atmos. Sci.* **47**: 1149–1162.

Moore RW, Montgomery MT. 2004. Reexamining the dynamics of short-scale, diabatic Rossby waves and their role in midlatitude moist cyclogenesis. *J. Atmos. Sci.* **61**: 754–768.

Moore RW, Montgomery MT. 2005. Analysis of an idealized, three-dimensional diabatic Rossby vortex: A coherent structure of the moist baroclinic atmosphere. *J. Atmos. Sci.* **62**: 2703–2725.

Mooring TA. 2011. 'Changes in atmospheric eddy length with the seasonal cycle and global warming', Earth, Atmospheric, and Planetary Sciences dept. thesis. MIT: Cambridge, MA. http://hdl.handle.net/1721.1/65599; accessed 21 November 2017.

O'Gorman PA. 2011. The effective static stability experienced by eddies in a moist atmosphere. *J. Atmos. Sci.* **68**: 75–90.

O'Gorman PA, Schneider T. 2008. The hydrological cycle over a wide range of climates simulated with an idealized GCM. *J. Clim.* **21**: 3815–3832.

O'Gorman PA, Schneider T. 2009. The physical basis for increases in precipitation extremes in simulations of 21st-century climate change. *Proc. Natl. Acad. Sci. USA* **106**: 14 773–14 777.

Parker DJ, Thorpe AJ. 1995. Conditional convective heating in a baroclinic atmosphere: A model of convective frontogenesis. *J. Atmos. Sci.* **52**: 1699–1711.

Pendergrass AG, Gerber EP. 2016. The rain is askew: Two idealized models relating the vertical velocity and precipitation distributions in a warming world. *J. Clim.* **29**: 6445–6462.

Pendergrass AG, Hartmann DL. 2014. Changes in the distribution of rain frequency and intensity in response to global warming. *J. Clim.* **27**: 8372–8383.

Perron M, Sura P. 2013. Climatology of non-Gaussian atmospheric statistics. *J. Clim.* **26**: 1063–1083.

Pfahl S, O'Gorman PA, Singh MS. 2015. Extratropical cyclones in idealized simulations of changed climates. *J. Clim.* **28**: 9373–9392.

Raymond D, Jiang H. 1990. A theory for long-lived mesoscale convective systems. *J. Atmos. Sci.* **47**: 3067–3077.

Rotunno R, Muraki DJ, Snyder C. 2000. Unstable baroclinic waves beyond quasigeostrophic theory. *J. Atmos. Sci.* **57**: 3285–3295.

Sardeshmukh PD, Compo GP, Penland C. 2015. Need for caution in interpreting extreme weather statistics. *J. Clim.* **28**: 9166–9187.

Shi X, Durran D. 2016. Sensitivities of extreme precipitation to global warming are lower over mountains than over oceans and plains. *J. Clim.* **29**: 4779–4791.

Simmons AJ, Hoskins BJ. 1976. Baroclinic instability on the sphere: Normal modes of the primitive and quasi-geostrophic equations. *J. Atmos. Sci.* **33**: 1454–1477.

Snyder C, Lindzen RS. 1991. Quasi-geostrophic wave-CISK in an unbounded baroclinic shear. *J. Atmos. Sci.* **48**: 76–86.

Tamarin T, Kaspi Y. 2016. The poleward motion of extratropical cyclones from a potential vorticity tendency analysis. *J. Atmos. Sci.* **73**: 1687–1707.

Valdes PJ, Hoskins BJ. 1988. Baroclinic instability of the zonally averaged flow with boundary layer damping. *J. Atmos. Sci.* **45**: 1584–1593.

Wernli H, Dirren S, Liniger MA, Zillig M. 2002. Dynamical aspects of the life cycle of the winter storm 'Lothar' (24-26 December 1999). *Q. J. R. Meteorol. Soc.* **128**: 405–429.

Whitaker JS, Davis CA. 1994. Cyclogenesis in a saturated environment. *J. Atmos. Sci.* **51**: 889–907.

Zurita-Gotor P. 2005. Updraft/downdraft constraints for moist baroclinic modes and their implications for the short-wave cutoff and maximum growth rate. *J. Atmos. Sci.* **62**: 4450–4458.